Dynamic Equilibrium in the Cetyltrimethylammonium Bromide-Au Nanoparticle Bilayer, and the Consequent Impact on the Formation of the Nanoparticle Protein Corona

Dynamic equilibrium in the CTAB - Au nanoparticle bilayer, and the consequent impact on the formation of the nanoparticle protein corona.

Francesco Barbero†‡, Oscar H. Moriones†‡, Neus G. Bastús†, *Victor Puntes†‡§‖

† Catalan Institute of Nanoscience and Nanotechnology (ICN2), CSIC and BIST, Campus UAB, Bellaterra, 08193 Barcelona, Spain

‡ Universitat Autònoma de Barcelona (UAB), Campus UAB, 08193, Bellaterra, Barcelona, Spain

§ Vall d'Hebron Institut de Recerca (VHIR), 08035, Barcelona, Spain

‖ Institució Catalana de Recerca i Estudis Avançats (ICREA), P. Lluís Companys 23, 08010 Barcelona, Spain

Keywords

CTAB, gold nanoparticles, gold nanorods, dynamic equilibrium, protein corona, phase transfer

Abstract

Nanoparticles in ionic solutions are usually surrounded by stabilising molecules that avoid aggregation and determine their surface properties, highly influencing their behaviour. The present work aims to shed light on the static *vs* dynamic nature of the CTAB bilayer on top of gold nanoparticles, and to understand its consequences on nanoparticle evolution in biological scenarios. A systematic study of the CTAB bilayer of Au nanorods and nanospheres was carried out, exploring the role of the excess of free surfactant in solution on nanoparticles surface properties and colloidal stability. Results indicated the presence of a CTAB bilayer where the external layer is in rapid dynamic equilibrium with the free surfactant in solution. The internal surfactant layer of the gold nanospheres was found to be also in dynamic equilibrium. Conversely, the gold nanorods showed a permanent internal layer. As a consequence, CTAB-nanoparticle dispersions always contain free CTAB in excess in order to maintain NPs colloidally stable. Otherwise, decreasing the free CTAB concentration results in nanoparticle aggregation. The impact of the dynamic equilibrium on the particles exposure to biological fluids and on the formation of the nanoparticles' protein corona was studied, observing different fates of the nanoparticles depending on the amount of free CTAB in solution.

Introduction

Nanoparticles (NPs) because of their numerous outstanding physical and chemical properties [1, 2] are used in a wide variety of applications including catalysis [3], sensing [4], photovoltaics [5] and biomedicine [1]. NPs are usually capped by surfactant molecules that provide repulsive forces to prevail over the attractive ones to which NPs are subject [6]. These surfactants highly influence the NPs' surface features which determine interactions with their surroundings. Consequently, by just changing the type and concentration of these surfactants it is possible to modulate NP behaviour and design their surface for specific applications [7]. Several types of interactions occur between NPs and surfactants, depending on their chemical nature, from strong covalent bonds to weak Van der Waals interactions.

An important point is if the surfactants are permanently bound to the NP surface or in a dynamic equilibrium with free surfactant molecules present in solution. In the latter case, the removal of this excess of molecules in solution by purification or dilution leads to NPs aggregation [8]. In these conditions, complete purification of such NPs is not possible without compromising NP colloidal stability. Besides, surfactants in dynamic equilibrium allow for its exchange and further NP engineering. Consequently, from a biomedical and nano-safety point of view, dispersion of NPs in biological or environmental media will commonly lead to NP surfactant exchange and/or NP aggregation.

A widely used NPs surfactant is the cationic cetyltrimethylammonium bromide (CTAB) which in the case of Au can be also a shape-directing agent, widely employed for the synthesis of nanospheres [9], nanorods [10]; nanoprisms [11], nanocubes [10] and nanostars [12]. Furthermore, it is a surfactant typically used to confer cationic properties to AuNPs [13] and has been used as a positive control for toxic NPs in many nano-safety studies [14, 15], despite that the toxicity is associated to the excess of CTAB in solution [16, 17] rather than the Au-CTAB NPs.

CTAB is a quaternary ammonium surfactant that due to its amphiphilic nature, through the formation of micelles, it is dispersible both in water and in several organic polar and apolar solvents [18]. In pure water, CTAB presents a Krafft temperature of 23°C [19] and a critical micelle concentration (CMC) of about 0.92 mM at 25°C in pure water [20, 21]. Evidently, the presence of different ions, macromolecules and NPs, shifts these critical concentrations to lower values [20]. Besides, at concentrations well above the CMC, approximately 300 mM, the CTAB micelles start to grow and

become rod-like in shape [22] what is used to template the growth of AuNPs. Note that the surfactant molecules in these micelles are in equilibrium with CTAB free in solution and at the air water interface [23].

Physicochemical characterization of CTAB layers on AuNPs have shown the formation of a cationic surfactant bilayer [24] and studies on Au nanorods (AuNRs) have shown that it has a thickness of 3,2±2nm with an alkyl chain density of 80-100%. The observed thickness is smaller than the extended alkyl chain length, opening the hypothesis of potential entanglement of the alkyl chains [25]. The first layer of the CTAB bilayer is bound to the AuNPs surface via electrostatic interactions of the cationic quaternary ammonium head group with an anionic NPs surface consisting of metal bromide complexes [26, 27].

Initially, these CTAB-AuNPs were found to be highly cytotoxic [28, 29], and the effective concentration required to reduce cell viability by 50% (EC50) was found to be between 2-30μM [28, 30]. However, it was observed later that the large amount of CTAB used to synthesize AuNPs, normally in the order of 100 mM, clearly interfered with biological processes [29]. Consequently, the CTAB stabilized AuNPs did not cause cytotoxicity to cultivated cells if they were previously purified by centrifugation, while the resulting supernatant displayed the toxicity previously shown in the non-purified sample [16, 17]. These works highlighted the need to purify CTAB stabilized AuNPs to study their biological impacts. However, purification of CTAB stabilized AuNPs induce loss of colloidal stability [8, 25, 31]. Consequently, further studies are required for a deeper understanding of the static *vs* dynamic nature of the CTAB bilayer and its consequences on NPs physicochemical properties and behaviour in biological scenarios.

In the present work, physicochemical characterization of the CTAB bilayer of gold nanospheres and gold nanorods was carried out, highlighting the presence of a dynamic equilibrium between the CTAB present in the NP bilayer and that free in solution. Then, the impact of the dynamic equilibrium on particles exposition to biological fluids and on the formation of NPs protein corona was studied.

Results and Discussion

In order to investigate the physicochemical properties of the CTAB bilayer and its static *vs* dynamic equilibrium, quasi-spherical CTAB-stabilized gold nanoparticles (AuNSs) and rod-like CTAB-stabilized gold nanoparticles (AuNRs) were chosen (Figure 1). These two shapes were selected as the most representative of the AuNPs family and because spheres present a high surface curvature while rods are rather flat. This influences the interaction between surfactant molecules in the bilayer. In addition to curvature radii, the different shapes have been shown to expose different crystal planes [32]. AuNSs are generally claimed as faceted multi-twinned structures with decahedral or icosahedral geometry, with all crystal faces exposing Au(111) planes [33, 34]. In the case of AuNRs synthesised in presence of CTAB and traces of $AgNO_3$, the described crystallographic analysis report Au(250) facets on the flat sides, and Au(111) and Au(110) facets on its tips [35]. It has been shown that silver is present mainly on the NP surface - feature that could influence the interaction with CTAB [26].

The AuNPs were synthesized following seeded-growth approaches using reported protocols [9, 10]. The physicochemical properties of CTAB stabilized NPs (AuNP@CTAB) and the nature of the CTAB bilayer were characterized by UV-Vis spectroscopy, Zeta potential analysis, Dynamic Light Scattering (DLS) and Scanning Transmission Electron Microscopy (STEM) analysis. This combination of characterization techniques provided a robust description of the NPs and their aggregation state.

As can be seen in Figure 1, bright field STEM images showed a good monodispersity of both NPs. AuNSs presented diameters of 9.5 ± 0.9 nm and AuNRs an aspect ratio of 2.7, corresponding to average dimensions of 42.3 ± 4.5nm x 15.7 ± 3.2nm. The UV-Vis spectra showed typically localized surface plasmon resonance (LSPR) profiles [36]: a single peak for the AuNSs at 522.5nm and two peaks in the case of AuNRs at 515nm (transverse LSPR) and 652nm (longitudinal LSPR). After synthesis, the AuNPs concentration was $5.7*10^{12}$ NPs/ml for AuNSs (total surface area $1.6*10^{15}$ nm^2/ml) and $6.2*10^{11}$ NPs/ml for AuNRs (total surface area $1.5*10^{15}$ nm^2, assuming a cylinder). CTAB concentrations of as-synthesized NPs were respectively 75mM and 100mM In these conditions the Z potential values were found to be +38.0±7.3 mV (conductivity 2.4mS/cm) for the AuNSs and +46.9±2.3 mV (conductivity 3.0mS/cm) for the AuNRs. The intensity of scattering of AuNPs was at least 6 times higher than CTAB solutions at the same concentration, confirming that the measured values were due only to the NPs and not a significant superimposition of surface charge values of free CTAB micelles and AuNPs.

First, we investigated the mechanism of the AuNP@CTAB colloidal stability. The two types of NPs were exposed to increasing concentrations of NaCl (from 250 mM to 1500 mM, final concentrations) maintaining the total surface area of NPs constant in all the different samples. Samples were diluted in order to obtain the same final CTAB concentration of 57 mM. NP colloidal stability was assessed by UV-Vis spectroscopy and the Z potential was monitored for all the samples (Figure 1 C-F). As expected, with an increase in ionic concentration, the Z potential decreased, reaching values below +30 mV already at 250mM of NaCl and just slightly positive after 500 mM (~ +8 mV). The UV-Vis spectra profiles of the samples exposed to the salt solutions did not show any changes ascribable to a loss of stability and consequent aggregation and sedimentation, even at 1500mM of NaCl. In the case of mere electrostatic repulsion between particles, DLVO theory claims that a Z potential larger than around ±30 mV is needed to sustain colloidal stability [37, 38]. As in these really high ionic concentrations, electrostatic charges are efficiently screened, it can be concluded that AuNP@CTAB presents a steric stabilizing component that prevents NPs from aggregation since steric stabilization is independent of ionic concentration [38]. Note that the presence of abundant free CTAB micelles could determinately contribute to the observed stability. Unfortunately, *vide infra*, purification leads to NP aggregation by alteration of the external CTAB bilayer, so we cannot answer this question.

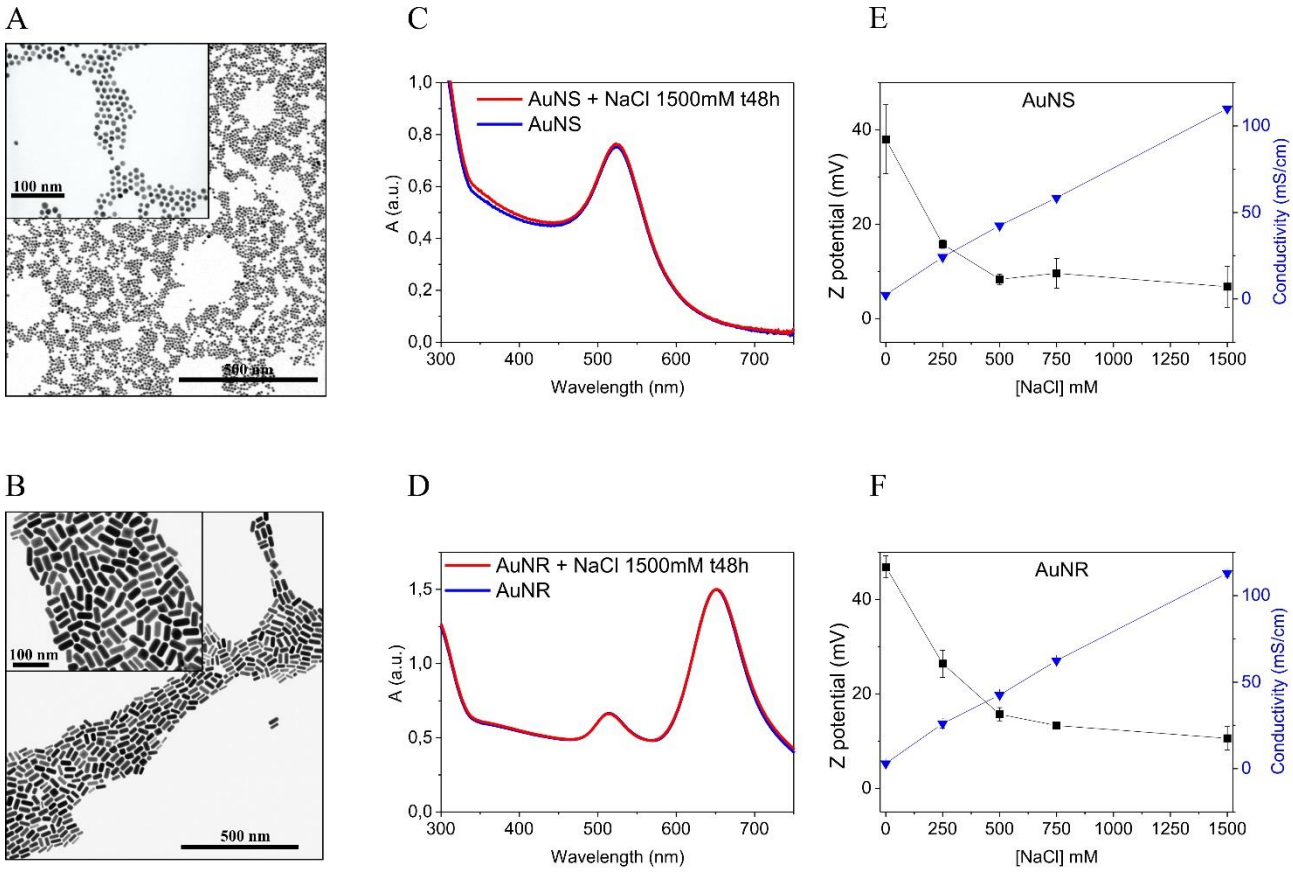

Figure 1. Physicochemical characterization of the AuNPs and steric stabilizing property of the CTAB AuNS and AuNR bilayer. (A, B) Bright field STEM images of AuNS (9.5±0.9nm) and AuNR (42.3±4.5nm x 15.7±3.2nm); (C) UV-Vis spectra of AuNS, CTAB 57mM (Blue) and AuNS, CTAB 57mM NaCl 1500mM after 48h (Red); (D) UV-Vis spectra of AuNR, CTAB 57mM (Blue) AuNR, CTAB 57mM NaCl 1500mM after 48h (Red); (E) Z potential (■) and conductivity (▼) of AuNS with growing concentrations of NaCl, concentration of NPs were the same in all samples. (F) Z potential (■) and conductivity (▼) of AuNR with growing concentrations of NaCl, the concentration of NPs were the same in all samples.

After synthesis, the colloidal solutions presented a really high CTAB concentration (75 and 100 mM respectively). Performing a theoretical calculation of the amount of CTAB molecules needed to form a bilayer on top of the NP, we found concentration values between ~ 8-15 μM for the spheres (< 0.02 %) and ~ 8 μM for the rods were found (~ 3.1-5.7 and 3.1 CTAB molecules per nm^2 respectively, see materials and methods). These calculations indicate that the CTAB present after the synthetic procedure is in really large excess in comparison with the surfactant forming the bilayer on top of the NP surface. As CTAB presents an EC50 between 2-30μM [28, 30], its concentration in the AuNPs samples has to be reduced by at least 6 orders of magnitude to avoid cytotoxicity. However, as it has been reported, the purification of AuNP@CTAB leads to a destabilization of the NPs [25, 31].

The physicochemical characterization of the AuNS and AuNR along of a systematic purification was carried out. AuNPs were purified by simple centrifugation, supernatant removal, and further re-suspension. In, each washing step, 90% of the supernatant was removed and the pellets reconstituted to the initial volume with mQ water. Volumes were checked using an analytical balance. With this procedure, in each washing step the amount of free CTAB was reduced by 90%. Table 1 reports the free CTAB concentrations at the net of the theoretical CTAB bilayer. The CTAB concentrations were confirmed with a quantification colorimetric assay (see materials and methods). Of note, after the third washing step, the concentration of CTAB was lower than its CMC (0.9 mM in mQ water at RT).

	Free CTAB (mM)			
Centrifugal Washing Step (90%)	**AuNS**		**AuNR**	
Before Wash (**BW**)	75	*74.5±0.1*	100	
After 1 centrifugal Wash (**A1cW**)	7.5	*7.448±0.01*	10	
After 2 centrifugal Wash (**A2cW**)	0.8	*0.745±0.007*	1	~ CMC
After 3 centrifugal Wash (**A3cW**)	0.08	*0.071±0.005*	0.1	
After 4 centrifugal Wash (**A4cW**)	0.008	*0.013±0.003*	0.01	~ EC50

Table 1. Concentration of free CTAB after several centrifugal washing steps, theoretical and measured (*italic*) values.

In order to monitor the washing process, physicochemical characterization of the samples after each purification step was performed. For both AuNPs, until the third centrifugal wash step (A3cW), samples did not present any problems in being re-suspended (Figure 2). However, after the fourth wash (A4cW), it was not possible to re-disperse a significant part of the pellets (Figure 2B, E images). Consequently, it was not possible to perform a fifth washing step. The UV-Vis spectra showed a progressive decrease in the absorbance after each step, just partially ascribable to a normal loss of NPs (c.a. 5%) during the purification process (Figure 2A, D). Interestingly, after each wash, a reproducible and not negligible blue-shift of the LSPR was observed (Figure 2A-B, D-E), AuNSs from 522.5nm to 518nm, and in AuNR from 652nm to 646nm which can be ascribable to a decrease in the degree of the packaging of the CTAB molecules at the surface of the NPs.[39]. In AuNRs the blue-shift was observed only for the longitudinal LSPR [40] which is more sensible that the transverse one to changes in the dielectric media around the NPs. After the fourth wash, the UV-Vis spectrum of the AuNSs showed an increase of the background, an indication of aggregation, and the AuNRs spectrum showed a broadening of the longitudinal band and the maximum 15nm red-shifted, also indicating aggregation [41]. Interestingly, if the AuNSs A4cW was re-suspended in a solution of CTAB 75mM instead of mQ water, the LSPR maximum was 522.5nm, the same as the not purified sample (Figure 2B,E - Red squares). During the purification process, the Z potential measurements initially showed an increase in their values (A1cW) and a substantial decrease in the standard deviation of the measure. From the seconds washing steps (A2cW), the Z potential started to decrease even if the conductivity decreased. Thus, the Z potential of AuNSs dropped from +38.0±7.3 mV to +13.8±3.4 mV and for the AuNRs from +46.5±8.2 mV to +21.3±1.9 mV. Conductivity values decreased from 2.4 mS/cm to 0.004 mS/cm and from 3.8mS/cm to 0.004 mS/cm, respectively.

The loss in stability after four purification step together with the observed blue-shifts, associated with a decrease of the local Refractive Index (RI) [42, 43] and the Z potential decrease, indicating that the AuNP@CTAB are subjected to changes in their surface state throughout the purification process. To further evaluate the change in the NPs properties, a solution of NaCl (final NaCl concentration 250mM) was added to the washed samples in order to observe the steric stabilization described in the not purified AuNP@CTAB samples. NPs A1cW, A2cW, and A3cW did not present any sign of aggregation. Conversely, the UV-Vis spectra at time 0 after A4cW clearly showed the appearance of a second peak and a rising of the background, clearly indicating NP aggregation [41] (Figure 2A, grey dash). From these results, it seems that the observed aggregation after four purification steps is due to the observed loss in steric stabilization, which is related to the number and conformation of surfactant molecules absorbed at the NP surface. Here again, the decrease of the Z potential [44] and the LSPR

blue-shifts, could be due to a less dense CTAB bilayer [45]. The aggregation as CTAB concentration decrease and the recovering of initial NPs characteristic when re-suspended in a CTAB solution, indicates the bi-directional dynamic relationship between the excess of CTAB in the solution and the NP bilayer structure: reducing the surfactant in the solution means shifting the equilibrium to free CTAB in solution, thus reducing the CTAB forming the NPs bilayer.

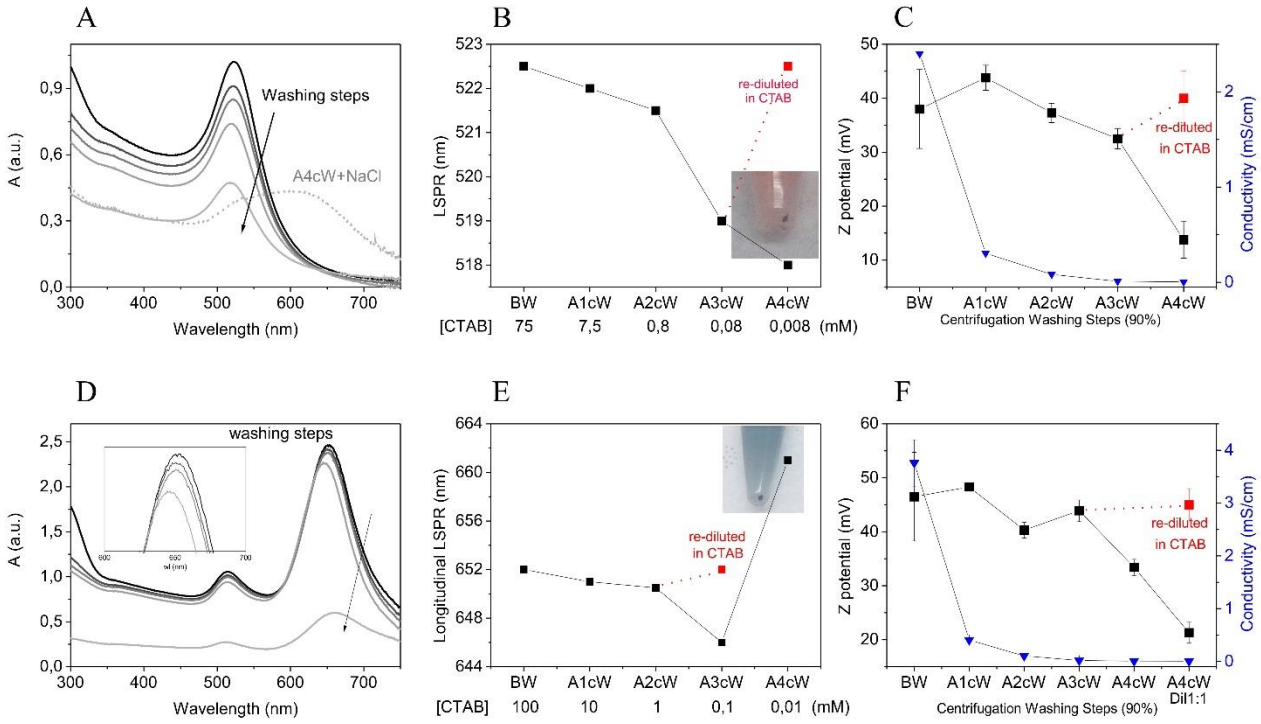

Figure 2. Physicochemical characterization of AuNS and AuNR after successive centrifugation washing steps. (A, D) UV-Vis spectra of AuNS and AuNR as synthesized and after different centrifugation purification/washing steps, in each stage 90% of the supernatant volume was removed and the samples were filled with an equal volume of mQ water, in grey dash the AuNS after four centrifugation wash (A4cW) exposed to NaCl 250mM. (B-E) LSPR value of AuNS and Longitudinal LSPR value of AuNR after each washing step (A*n*cW); the photos represent the samples after 4 washing steps and is possible to notice that the NPs pellets were not totally re-dispersable. (C, F) Z potential (■) and conductivity (▼) of AuNS and AuNR after each purification step.

To strengthen this hypothesis and to avoid possible effects due to the used "aggressive" purification method (centrifugation), alternative purification procedures were explored. Firstly, instead of removing 90% of the supernatant in the centrifugation procedure, 99% was removed in order to obtain the same final free CTAB concentration in just two steps at the expense of losing some AuNPs. In this case, very similar results to the A4cW were obtained (data not shown). "Milder" washing techniques were also explored. Diafiltration and classic dialysis against mQ water were used to purify AuNP@CTAB from the excess of the surfactant (Figure SI-1). Both techniques showed that after several purification steps, the NPs started to lose colloidal stability and the subsequent decrease in the Z potential was observed. Indeed, the gentlest method to shift the equilibrium towards the free CTAB

form was to directly dilute the AuNP@CTAB sample in mQ water, reaching the same surfactant concentrations obtained in the several centrifugation steps. Thus, samples were diluted 100 times and 1000 times in mQ water in order to obtain a concentration of free CTAB of respectively 0.08/0.1 mM (AuNS/AuNR) and 0.008/0.01 mM, corresponding to the A3cW and A4cW respectively, maintaining constant the number of NPs at the initial synthesis concentrations. As a control, the samples were also diluted in a water solution of CTAB 75mM. UV-Vis spectra of the AuNSs diluted 1000 times showed some extent of aggregation from time 0, translated into a shoulder around 680nm that rapidly evolved over time. At time 24h, the LSPR vanished, an indication of the complete aggregation of the NPs that led to sample sedimentation (Figure 3A). Conversely, the sample diluted 1000 times in the CTAB 75mM solution did not present any sign of aggregation neither after 24h, and it presented an LSPR at 522.5 nm as in the as synthesised sample (Figure 3A, red line). The AuNSs diluted 100 times presented an LSPR at 519nm (as the A3cW) and did not present any indication of aggregation after 24h (Figure 3 B). Also, in the sample diluted 100 times in CTAB 75mM, the LSPR was 522.5 nm and in this case is clearly appreciable also an increase in absorbance (Figure 3B, red line). All these results are indicative of the persistent equilibrium between CTAB free in solution and at the AuNP bilayer. The Z potential of the diluted AuNSs showed a decrease in the values similar to the one observed in the purification by centrifugation (Figure 3D). A concentrated NaCl solution was also added to the 100 times diluted AuNS (final concentration 250mM) and the sample was perfectly stable (Figure 3C). The same experiments were done on the AuNRs, and results are shown in Figure 3 confirming the same trends above described, with just a slower aggregation kinetic than sample diluted 1000 times.

These dilution experiments clearly show very similar results to those obtained with any of the purification procedures: loss in colloidal stability when the CTAB concentration was decreased; a progressive decrease in the Z potential as the free CTAB is removed; and a clear blue-shift in the UV-Vis spectra indicating a decrease surfactant concentration at the NP surface. Furthermore, the control samples diluted in a solution of CTAB 75mM showed the same characteristic of the not purified AuNP@CTAB samples, showing the same absorption profiles, Z potential and colloidal stability. Additionally, in control experiments, it was possible to appreciate that besides the difference in the LSPR maximum, higher values in the absorbance maximum were also observed, indicating other plasmonic evidence of a difference in the local RI [43].

The results show that a difference in the concentration of the free CTAB clearly affects the AuNP@CTAB surface and properties, and if the free CTAB concentration is re-established, the initial characteristic were also restored. It can, therefore, be confirmed that there is a reversible equilibrium

between the free CTAB and the bilayer CTAB. These results clearly indicate that diluting AuNP@CTAB does not mean obtaining solutions of the same particles just at different concentration, but solutions of different nano-objects that present a different surface and consequently, different properties.

These differences were observed along all the tested concentrations of free surfactant (100mM to 10μM) with prominent changes observed below the CTAB CMC. The possibility of purifying the samples one order of magnitude below the CTAB CMC seems to indicate that the presence of surfactant micelles in the solution is not required to have a colloidally stable AuNP@CTAB solution. However, the complete purification of the NPs from the free CTAB seems impossible. In other words, any stable dispersion of NPs in CTAB contains a toxic amount of free surfactant.

Interestingly, similar results were obtained with AuNS and AuNR, despite presenting different crystalline facets and surface curvatures. Consequently, despite the different packing of the bilayers on a flat or curved surface and a different preferential CTAB binding for different crystal facets, as postulated in literature [46], do not strongly affect the surfactant dynamic equilibrium, suggesting that these effects are related to the first monolayer, in contact with the Au (and Ag traces) surface, while the equilibrium of the second layer is rather independent of shape.

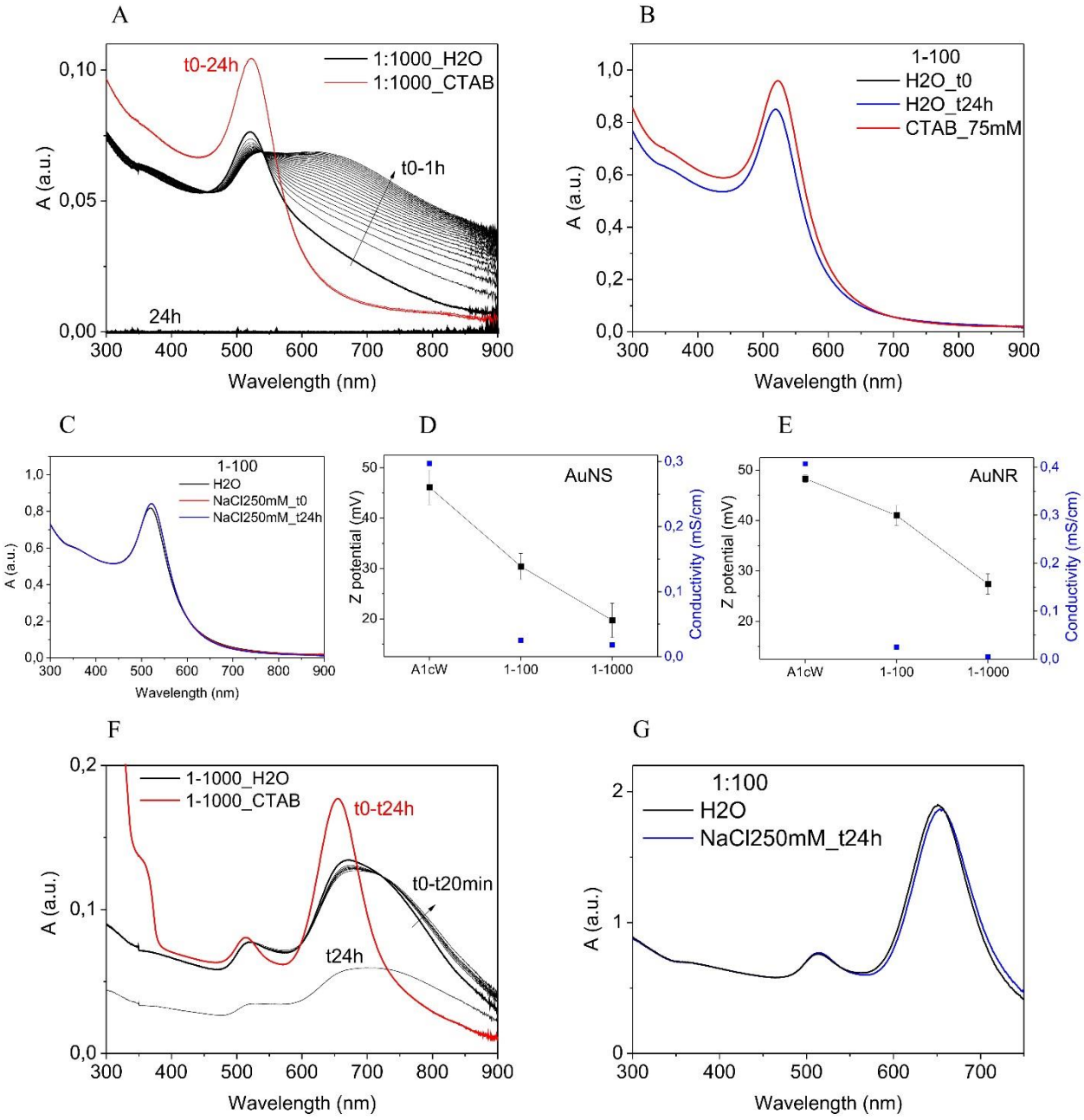

Figure 3. Comparison of physicochemical properties of AuNS and AuNR once diluted, under the CTAB CMC in mQ water or in a CTAB solution. (A) Time evolution of UV-Vis spectra of AuNS concentrated 100 times (CTAB 7.5mM): diluted 1:1000 (CTAB 8µM) in mQ water (Black) and in 75mM CTAB (Red). (B) Time evolution of UV-Vis spectra of AuNS concentrated 100 times (CTAB 7.5mM): diluted 1:100 (CTAB 80µM) in mQ water (Black) and in 75mM CTAB (Red). (C) UV-Vis spectra overtime of the previous sample diluted 1:100 exposed to 250mM NaCl. (D) Z potential (■) and conductivity (■) of AuNS diluted 1:1000 and 1:100 in mQ water. (E) Z potential (■) and conductivity (■) of AuNR concentrated 100 times (CTAB 10mM): diluted 1:100 and 1:1000 in mQ water. (F) Time evolution of UV-Vis spectra of AuNR concentrated 100 times (CTAB 10mM): diluted 1:1000 (CTAB 10µM) in mQ water (Black) and in 100mM CTAB (Red). (G) Time evolution of UV-Vis spectra of AuNR concentrated 100 times (CTAB 10mM): diluted 1:100 (CTAB 100 µM) in mQ water (Black) and in 250mM NaCl (Blue).

Regarding the structure of the CTAB bilayer formed on top of the AuNPs, the first layer, the internal one, has the polar head bound via chemisorbed bromide counterions, exposing the hydrophobic chain towards the solution [26, 27]. In contrast, the second layer, the external, is stabilized by hydrophobic interactions between the alkyl chains. The difference between the two types of interactions leaves the doubt that only the external layer, with a nature similar to that of micelles, could be in a dynamic equilibrium with the free CTAB. In this case, the observed aggregation could be also driven by a partial hydrophobic nature of the AuNP@CTAB single layer.

In order to try to assess this, AuNSs at the different purification steps were put in contact with two organic solvents with different polarity, 1-Octanol, used as a standard to measure the partition coefficient [47], and the more apolar Chloroform; in both solvents CTAB is soluble through the formation of reverse micelles [48]. The idea was to evaluate the ability of AuNP@CTAB to perform a phase transfer, being able to present just the first layer exposing the lipophilic alkyl moieties and consequently soluble in an organic solvent. Firstly, AuNSs were mixed with 1-Octanol (1:2) and observed for several days (Figure SI-2). None of the NPs were able to migrate, even partially, to the organic solvent. The A4cW sample started to aggregate almost immediately, and the A3cW began to present signs of aggregation after a few minutes. After 2 hours, the sample showed large AuNPs aggregates. The other samples did not show any change over time. This experiment just demonstrates another CTAB purification strategy, free CTAB was partitioned between water and the organic solvent and the free surfactant was reduced.

Besides, in the Water/Chloroform partition (1:2) of AuNSs, samples did not show any migration for the not purified particles (BW), A1cW and A2cW (Figure 4A). Interestingly, 4 days after the mixing with the $CHCl_3$, the A3cW migrated to the organic phase while the A4cW did not. UV-Vis spectra confirmed the observations and showed that the sample transferred to chloroform (AcW3) migrated completely and did not present any sign of aggregation (Figure 4B, C). It could be speculated that the A4cW, already at the limit of colloidal stability, was quickly destabilized due to removal of a little quantity of free CTAB by migration to the $CHCl_3$ phase and immediately aggregated losing the ability to phase transfer. In contrast, the A3cW, presenting 10 times free CTAB was more slowly destabilized by the removal of CTAB and before aggregating occurred NPs were able to undergo phase transfer into the $CHCl_3$ where the NPs are stable, indicating the possibility of having lipophilic AuNP@CTAB with just the first layer.

Taking advantage of the possibility of CTAB to solubilise the AuNPs in organic solvents, exploiting the salting-out effect [49], a saturated solution of NaCl was added to the AuNSs BW, A1cW, and A2cW that had been previously put in contact with a $CHCl_3$ phase. Immediately after vigorous mixing, all the NPs completely migrated into the organic phase (Figure 4D). The same strategy was tried with AuNRs and larger AuNSs with a diameter of 50nm. In both cases it was not possible to perform the phase transfer into the organic solvent, highlighting how a really small size is needed to pass through such interphase [50].

Another method was developed to perform a phase transfer of AuNRs. A solution of AuNRs (BW) was dried under mild vacuum (the dried powder presented a black colour) and $CHCl_3$ was subsequently added. A stable colloidal solution in organic solvent was obtained indicating a certain degree of aggregation (by UV-VIS), likely due to the drying procedure, as in the used method of solvent evaporation-induced assembly [36]. In order to avoid that aggregation, the polymer polyvinylpyrrolidone 360KDa (PVP) was added to the AuNRs solution before the drying procedure, as a thickener (final concentration 2.7 mg/ml). The solution was dried (the dried powder presented a green/blue colour) and re-suspended in $CHCl_3$ and a green/blue solution was obtained. The resultant UV-Vis spectrum presented the typical AuNRs profile, just red-shifted in comparison to the NPs dispersed in water, an effect ascribable to the increase in the RI of the organic solvent [51] (Figure 4F). The AuNRs in chloroform were stable over time (at least two weeks). A ligand exchange between CTAB and PVP could be ruled out as AuNSs coated with PVP experienced surfactant exchange when exposed to a CTAB solution (Figure SI-3), probably due to stronger interactions of the quaternary ammonium head group of the CTAB and the metal bromide complexes at the NP surface compared to a weaker interaction of Au and the PVP cyclic amide group.

The methods outlined above allowed the study of the dispersion of AuNPs in organic solvents with a CTAB monolayer. Note that stable AuNPs in organic solvents are required for various applications such as preparing hydrophobic composites with water-insoluble polymers and to control assembly of nanoparticles on substrates upon evaporation from volatile solvents [52-54].

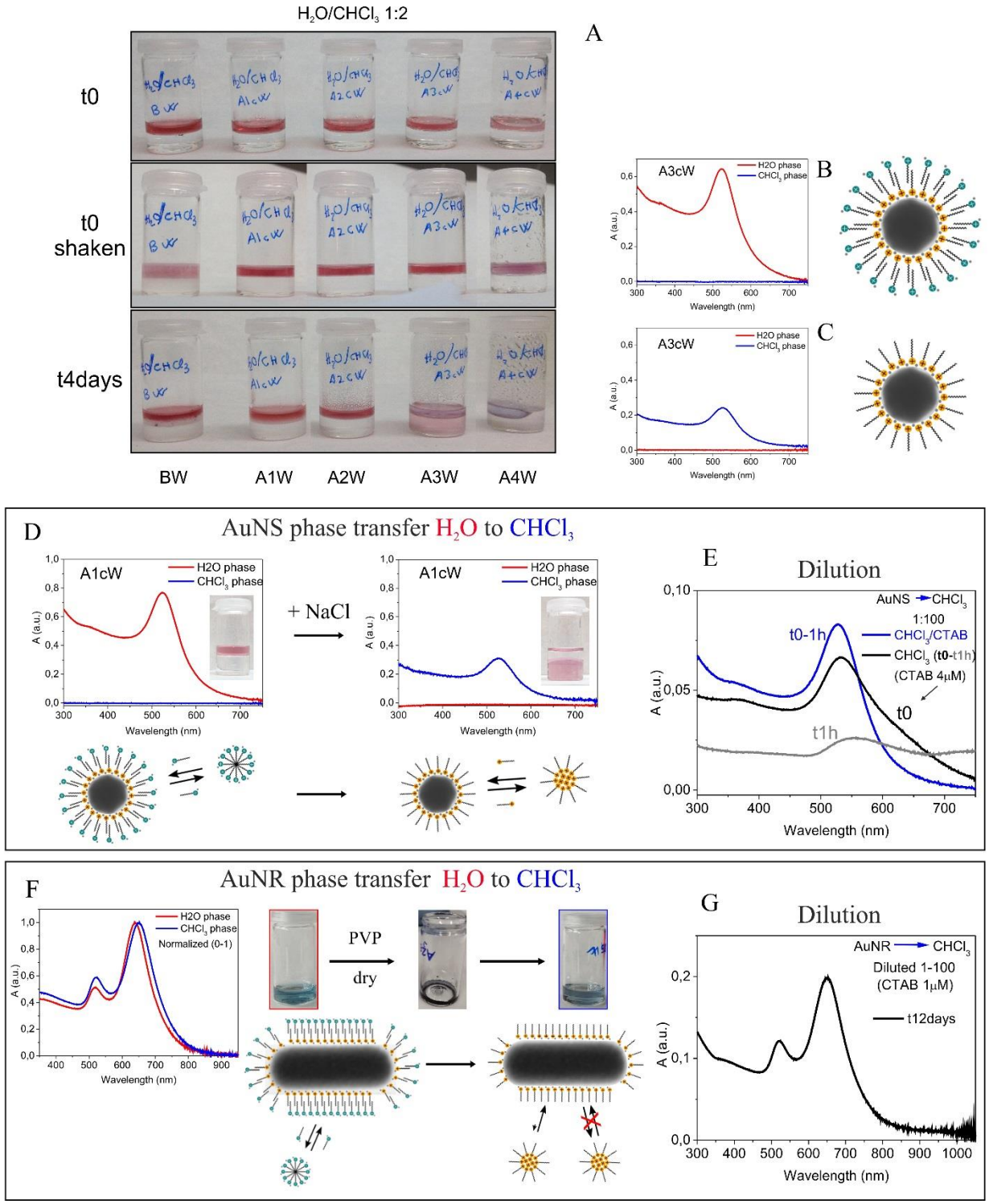

Figure 4. Nature of the internal CTAB layer. (A) Time evolution of Water/Chloroform partition experiment: 1 ml of each AuNS at the different washing steps have been exposed to 2 ml of $CHCl_3$. (B) UV-Vis spectra, at time 0, of the water phase (Red) and $CHCl_3$ phase (Blue) of AuNS A3cW (CTAB ~ 0.08mM). (C) UV-Vis spectra, after four days, of the water phase (Red) and $CHCl_3$ phase (Blue) of AuNS A3cW (CTAB ~ 0.08mM). (D) AuNS phase transfer: UV-Vis spectra and images of the sample A1cW added of a satured NaCl solution, mixed with $CHCl_3$. (E) Time evolution of UV-Vis spectra of AuNS A1cW concentrated 100 times migrated to $CHCl_3$ (1:20, CTAB 0.4mM): diluted 1:100 in $CHCl_3$+CTAB 100mM (Blue) and in pure $CHCl_3$, final CTAB 4μM (Black, Grey). (F) AuNR phase transfer: UV-Vis spectra and images of the sample BW added of PVP, dryed and resuspended in $CHCl_3$. (G) Time evolution of UV-Vis spectra of AuNR A3cW concentrated 10 times migrated to $CHCl_3$ (CTAB 10μM): diluted 1:100 in $CHCl_3$+CTAB 100mM (red) and in pure $CHCl_3$, final CTAB concentration 1μM (Black, Grey).

Thus, it was possible to isolate AuNSs and AuNRs with only the first CTAB layer, and consequently, this allowed the study of its behaviour. The same dilution strategy was used to evaluate the influence of free CTAB, adding at the beginning a phase transfer step into $CHCl_3$. AuNS-A1cW sample concentrated 100 times (free CTAB ~7.5mM) was added to a saturated solution of NaCl and put in contact with $CHCl_3$ (1:20). Also at this high concentration of NPs, the migration to the organic solvent occurred completely without any sign of NP aggregation. The resultant solution (observed to be stable at least two weeks) was further diluted 1:100 into $CHCl_3$ (CTAB final concentration 0.004mM) and $CHCl_3$+CTAB (100 mM). The evolution of the two solutions was followed by UV-Vis spectroscopy (Figure 4E) as a function of time. The particles diluted into the chloroform solution of CTAB were clearly stable over time, conversely, the NPs diluted just in pure $CHCl_3$ presented after the dilution a shoulder around 650nm typical of the of NP aggregation that evolved over time, indication of a strong destabilization of the system in these conditions. These results showed how the different concentration of free CTAB also influences the colloidal stability of AuNSs in the organic solvent where the AuNP@CTAB present only the first layer, conferring them lipophilic properties. From these results, it could be possible to conclude that on the AuNSs, not only the external layer of CTAB is in dynamic equilibrium with the free surfactant but, at least in organic solvent, the internal layer is also dependent on the concentration of free surfactant, appearing to be also in dynamic equilibrium.

Then, PVP was added to AuNRs, A2cW and A3cW, concentrated 10 times (final free CTAB ~ 1mM and 0.1mM), dried and then re-suspended in the same volume of $CHCl_3$. Subsequently, the samples were diluted 100 times in $CHCl_3$ in order to obtain a final concentration of free CTAB around 10 μM and 1 μM (10 times less than the A4cW). Both solutions were stable for at least 12 days (Figure 4G). This result seems to indicate that in the organic solvent, the stabilizing CTAB layer is not significantly influenced by the free surfactant concentration, indicating that in the case of AuNR, at least in chloroform, the CTAB first layer is not in dynamic equilibrium, or the equilibrium is strongly displaced to the Au surface.

These findings seem to highlight that the interaction nature of CTAB forming the first layer on top of the gold surface is different when formed on AuNSs or on the AuNRs. The main differences lie in the surface curvature and the crystal facets of their sides, whereas NRs tips present a more similar nature to the AuNSs. Furthermore, AuNRs present silver atoms on the surface. The absence of a dynamic equilibrium of the AuNR CTAB first layer may result in a less accessible surface compared with AuNSs, and it can be imaged that behaves similar to the rod tips, supporting the hypothesis formulated in the literature, that CTAB adsorbs preferentially to the flat surface of rods rather than to its tips,

accepted to be one of the mechanisms underlying the rod anisotropic growth [46]. Consequently, it has been demonstrated that the end of the rods is much more reactive than the side [29, 36].

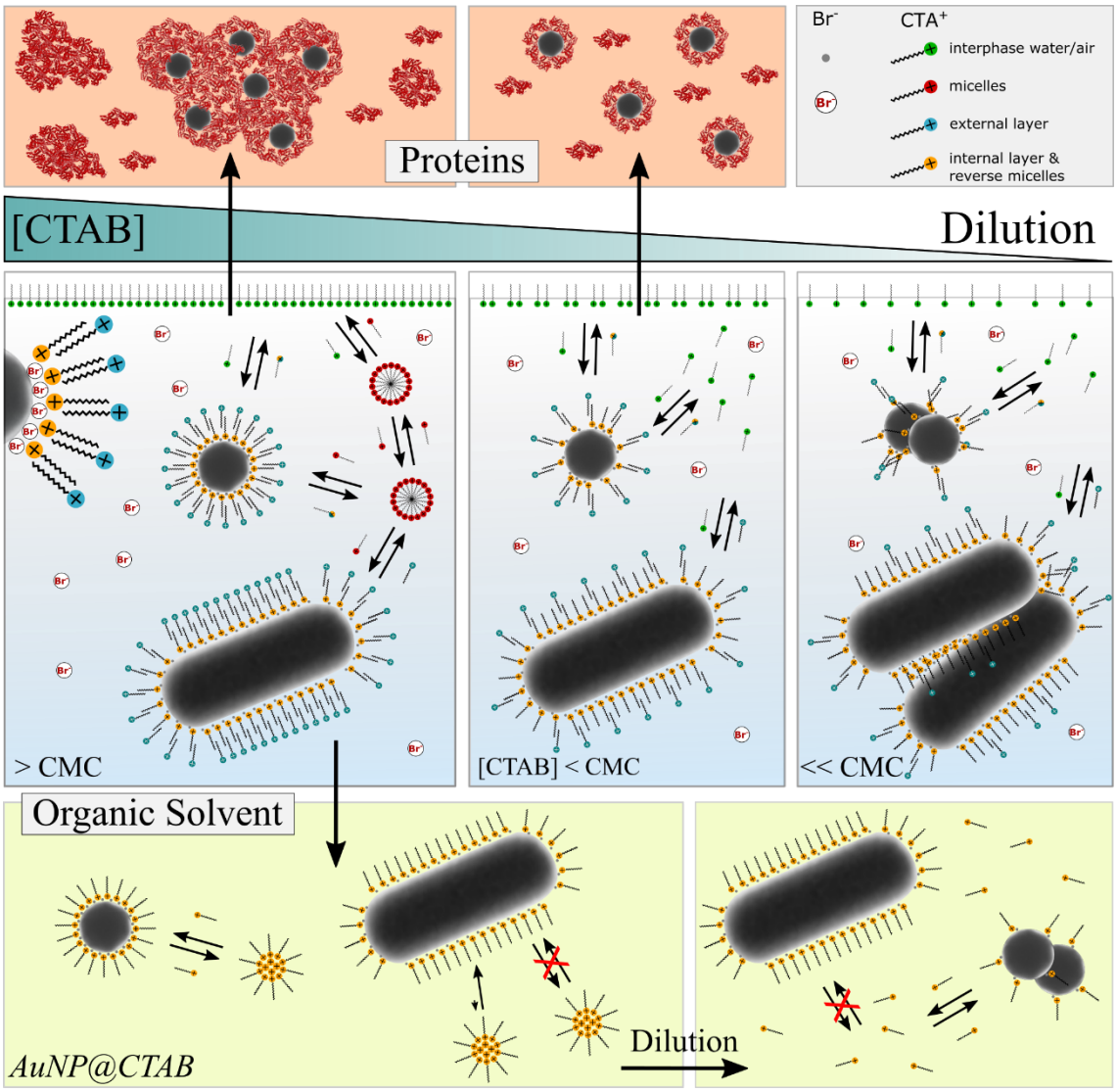

Figure 5. Scheme of the dynamic equilibrium in CTAB gold nanoparticles bilayer and its consequences on the NPs surface and colloidal stability. Impact on the formation of the NP protein corona and CTAB internal layer characterization by phase transfer strategy.

From a safety or bio-application point of view, NPs can unintentionally or intentionally enter living systems [55, 56]. Thus, the study of the interaction of NPs with biological systems is important to ensure their safe application and to understand their mechanism of interaction as medical tools. An important phenomenon that happens when NPs encounter biological fluids is the formation of a Protein Corona (PC) enveloping the NP. This is relevant, as it provides the biological identity of the NPs that come into contact with a living system mediating the interactions with cells and biological barriers, what has important implications on safety, biocompatibility and the use of NPs in medicine [57-62].

Previous studies have already shown the ability of AuNP@CTAB to undergo PC formation [17, 63, 64], and partial unfolding of the proteins composing the corona has also been reported [63, 65, 66]. In light of the previous results, AuNSs at the different washing steps were exposed to a common cell culture media in order to study the PC formation.

The five NP samples plus an aqueous solution of CTAB 8mM were diluted 1:10 in RPMI cell culture medium supplemented with 10% foetal bovine serum (FBS, as the source of proteins) and in just the RPMI without serum as a control. The dilution 1:10 obviously reduced the free CTAB of each sample in the final media. RPMI is a complex medium composed mainly of inorganic salts (0.138M), vitamins, amino acids, and sugars. The UV-Vis of the samples BW, A1cW, and A2cW did not show any significant differences once diluted to RPMI. After 22 hours of exposure, all three samples showed the comparison of a shoulder at approximately 600 nm due to the presence of AuNPs aggregates (Figure 6A, B). Correspondingly, the Z potential decreased over time, but still presented positive values (Figure 6C). In contrast, the A3cW and A4cW already at time 0 presented a large broadening of the LSPR, an increase of the baselines and a change in the colour of the solution from reddish to violet-blue, evidencing AuNPs aggregation (Figure 6A). After 22 hours the plasmonic profiles were totally lost and a black precipitate appeared (picture, Figure 6B). The aggregation of the A3cW and A4cW was totally expected as the RPMI presented a high salinity and, as described above, these samples had lost their steric stabilization. Conversely, the slow aggregation over time of the BW, A1cW, and A2cW was less expected, as previous experiments clearly showed that at that concentration of free CTAB, the cationic bilayer stabilized the NPs against aggregation, even in saline media ten times more concentrated. Looking at the composition of the RPMI, besides salts, vitamins, sugars, and amino acids are also present, and the majority of these molecules present chemical moieties able to interact with gold surfaces, especially the ones presenting –SH group such as cysteine, or interfere with the double bilayer. The partial replacement could be in line with the modest decrease observed in the Z potential. The possibility of the formation of a destabilizing additional layer of media molecules on top of the CTAB bilayer seems less likely as the Z potential should decrease more.

When proteins were added to the RPMI, the UV-Vis spectrum presented an increase in the absorbance in the UV region due to the presence of numerous organic molecules and macromolecules, and a shoulder at ~ 406 nm due to the presence of the hemoglobin in the FBS [67]. Once the 8mM CTAB solution was diluted 1:10 to RPMI+FBS, the UV-Vis spectrum presented a considerable increase in its absorbance that further increased over time and the solution became cloudy (Figure 6D). This result is in line with the reported ability of CTAB to unfold proteins [68]. Once unfolded, proteins tend to

aggregate [69], hence scattering light ("absorbing") at longer wavelengths (>600 nm). This explains the rising of the UV-Vis spectrum in samples BW and A1cW, and being less intense, in A2cW (Figure 6E, F). The presence of large aggregates in the three samples was also observed by Dynamic Light Scattering (data not shown). No signs of AuNPs aggregation in the absorbance profile were observed. The solutions were still reddish even if cloudy. Interestingly, after 22 hours the BW spectrum did not present any plasmonic feature in solution, but the samples had a reddish precipitate (Figure 6E). This result seems to suggest the formation of large proteins aggregates trapping the AuNPs, not in contact between them, so maintaining their individual plasmon resonance, forming a kind of proteins-AuNPs red composite. Z potential of these samples presented values of about -10 mV, similar to the CTAB solution diluted in RPMI+FBS, attributable to the proteins in solution. Note that Z potential is not sensitive to the degree of aggregation, thus, if different aggregates end up coated by proteins, all of them will display a similar surface charge. In the presence of FBS, A3cW and A4cW did not present any sign of aggregation and were stable over time (Figure 6G, H). Therefore, it was possible to purify them without concurring in NPs aggregation whether re-suspended in mQ water or in RPMI. The Z potential of both samples passed from positive to negative and these values were maintained after purifying the samples (Figure 6I), whether re-diluted in mQ water or in RPMI. In RPMI, the values were less negative as the conductivity was higher, and the values were very similar to the Z potential of the serum proteins. Furthermore, the LSPRs of the A3cW and A4cW presented red-shifts of ~ 2 nm after the exposition to the RPMI+FBS, ascribable to an increase of the local RI by the protein coating. DLS analysis showed an increase of the diameter of the particles of about 15nm not ascribable to NP aggregation. All in all, these results indicate the formation of a stabilizing PC on top of these particles, strengthened by the increase of the hydrodynamic diameter with a value ascribable to a protein monolayer. The possibility of purifying them without compromising their stability and the Z potential is a clear indication of the formation of a hard PC [70, 71].

Remains open the question as to whether, after the PC formation, in the A3cW and A4cW samples the CTAB is still present or undergoes ligand exchange. In any event, the observed dynamic equilibrium also in the first layer of AuNSs could suggest that the CTAB is no longer on the surface of the NPs. This study is an example of how at different concentrations of the cationic surfactant, the AuNP@CTAB present different properties and consequently change their fate. It can be concluded that exposing AuNP@CTAB to cell culture media leads to the formation of different objects, depending on the concentration of CTAB at the NP surface. The presence of a dense CTAB bilayer on the AuNSs (BW, A1cW, and A2cW) and a free CTAB concentration higher of 10μM lead to the formation of unfolded protein agglomerates that includes the AuNSs. It has been also shown by circular

dichroism that the protein composing the PC of AuNP@CTAB are partially denaturated [63, 65, 66], although the results of this study question the role of the free CTAB in interpreting such results.

These findings should influence the design and interpretation of NPs toxicity tests. A simple tangible example can be the widely used cytotoxicity tests where sequential dilutions of the compound to be evaluated are carried out. The exposed particles would present different properties depending on the dilution, especially because the concentrations of interest for toxicity studies (around CTAB EC50), as shown, are in the range where the CTAB layer undergoes more prominent changes.

In the present study, it was evidenced that it is not possible to directly prepare pure AuNP@CTAB samples without an excess of surfactant. Indeed, to avoid aggregation of the NPs, a concentration of the surfactant in the range of the reported EC50 (2-30μ) is needed for standard NP concentrations, de facto impeding a direct measurement of the cytotoxicity of the mere CTAB stabilized AuNPs entangled from the free cationic surfactant. Interestingly, the ability of AuNPs presenting a low dense CTAB bilayer to form a hard protein corona, without leading to any aggregation could be exploited as a ligand exchange strategy to prepare bio-compatible AuNRs.

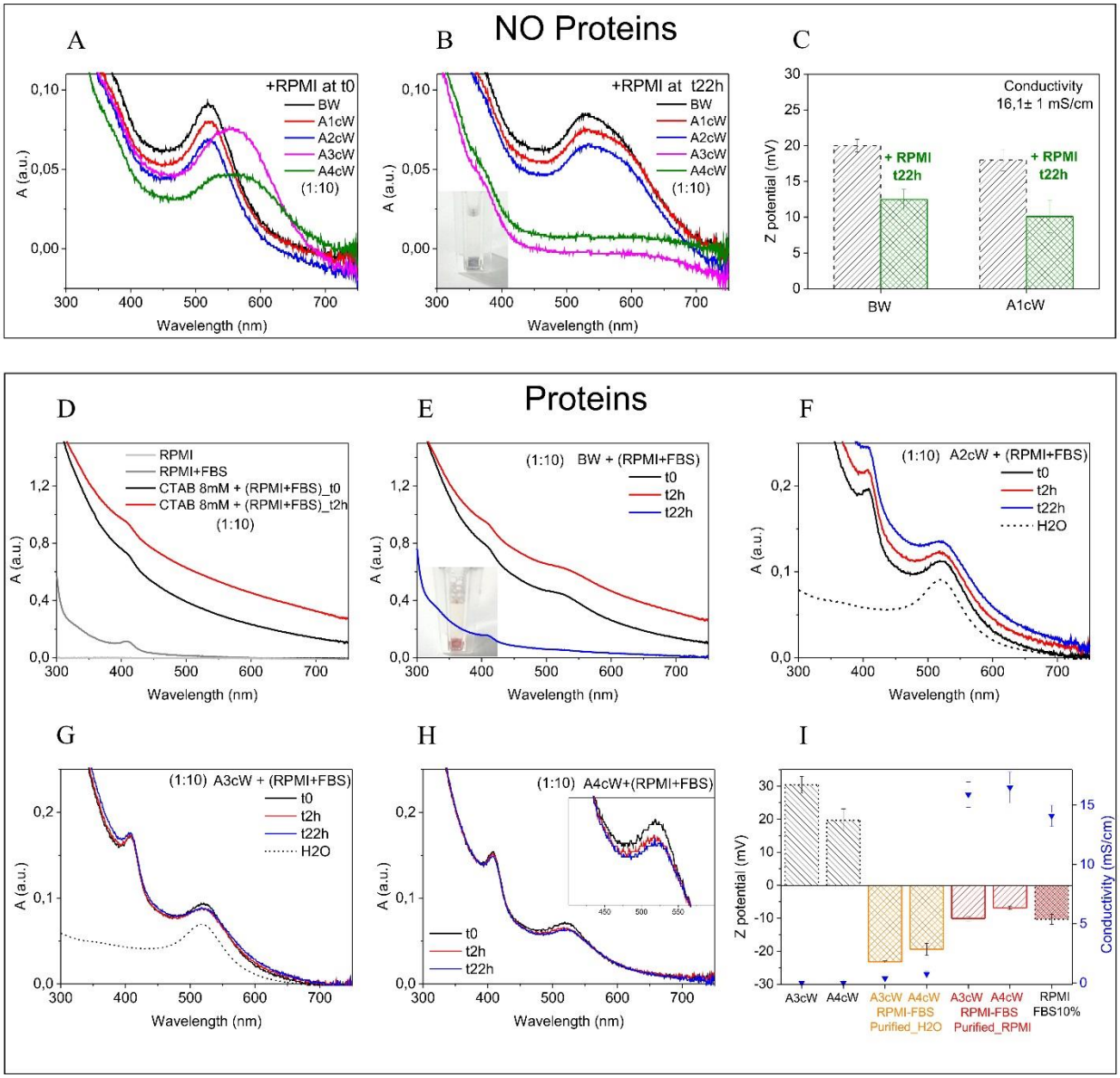

Figure 6. Exposition of AuNS to cell culture media (RPMI) and RPMI+10%FBS (A) UV-Vis spectra at time 0 of AuNS at the different step of purification/washing by centrifugation (CTAB ~ 75; 7.5; 0.8; 0.08; 0.008 mM) diluted 10 times into RPMI cell culture media. (B) UV-Vis spectra of the same samples after 22h of exposure at 37 °C; the photo shows the AuNS containing ~ 0.008mM CTAB (A3cW). (C) Z potential of AuNS BW, A1cW before (black lines) and after 22h exposure to RPMI (green rhombus). (D) UV-Vis spectra of: RPMI cell culture media, RPMI added of 10% Fetal Bovine Serum (FBS), 8mM CTAB diluted 1:10 into RPMI+FBS at time 0 and after 2h of incubation. (E) Time evolution (0-22h) of UV-Vis spectra of AuNS BW (CTAB 75mM) diluted 1:10 into RPMI added of FBS, the photo shows the AuNS after 22h. (F) Time evolution (0-22h) of UV-Vis spectra of AuNS A2W (CTAB 0.75mM) diluted 1:10 into RPMI added of FBS. (G) Time evolution (0-22h) of UV-Vis spectra of AuNS A3cW (CTAB 0.08mM) diluted 1:10 into RPMI added of FBS, plus control: AuNS A3cW diluted in mQ water at time 0. (H) Time evolution (0-22h) of UV-Vis spectra of AuNS A4cW (CTAB 0.008mM) diluted 1:10 into RPMI added of FBS. (I) Conductivity (Blue triangles) and Z potential of AuNS A3cW and A4cW (Black line); AuNS A3cW and A4cW exposed for 22h into RPMI added of FBS subsequently purified and re-suspended in water (orange rhombus) and in RPMI (red lines); RPMI added of FBS (red rhombus).

Conclusions

The results presented indicate the presence of a dynamic equilibrium between the CTAB bilayer at the NP surface and the free excess in solution. CTAB NP bilayer has a multiple, rather than a single nature, which has been shown to pass from providing a strong electro-steric stabilization to the NPs to not providing enough repulsive electrostatic force to prevail over the attractive one, leading to NP aggregation. This influences NPs fate once they are exposed to biological fluids, especially in respect of the formation of PCs. Moreover, obtaining a pure CTAB-NPs solution without the excess of free surfactant seems not possible, because due to the restoration of the equilibrium, free surfactant will be provided by the surfactant bilayer until NPs aggregation. The influence of the observed multiple nature of the CTAB bilayer on the interaction of the NPs with proteins could be exploited as ligand exchange strategy to prepare bio-compatible AuNR. The physicochemical characterizations of the surface properties of CTAB stabilized AuNPs performed in this study will allow better handling of this family of NPs and improve understanding of their behaviour in complex media. Specifically, it further highlights the importance of discriminating between the static and dynamic nature of NP coatings for the future development and biological and environmental exposure modelling of NPs.

Materials and Methods

Chemicals. Tetrachloroauric(III) acid trihydrate (99.9% purity), sodium citrate tribasic dihydrate (≥99%), ascorbic acid, $NaBH_4$, NaCl, cetyltrimethylammonium bromide (CTAB), chloroform, 1-octanol, 360KDa polyvinylpyrrolidone (PVP), $NaNO_3$, Sodium Hydroxide and RPMI-1640 (R7509) (with sodium bicarbonate, without L-glutamine and phenol red, liquid, sterile-filtered, suitable for cell culture) were purchased from Sigma-Aldrich. Fetal Bovine Serum, FBS (research grade, triple 0.1 micron filtration) was purchased from ThermoFisher scientific. Bromophenol blue sodium salt was purchased from J. T. Baker. All reagents were used as received without further purification. For all the studies with biological fluids, plastic material was sterile grade and all glass material was sterilized in an oven prior to use, autoclave sterilized Milli-Q water was used in the preparation of all solutions. **Nanoparticle Synthesis**. AuNPs were synthesized following the seeding growth approaches using the reported protocols developed by C. Murphy and co-workers [9, 10]. **Systematic NPs purification by centrifugation.** Centrifugation washing steps were performed at 34000g*30 min, 26°C for the AuNS and at 6000g*15min, 26°C for the AuNR. In each step, 90% of the supernatant was removed and the sample was reconstituted to the initial volume with mQ water. The volumes were checked using an

analytical balance. With this procedure in each washing steps the amount of free CTAB was reduced to 90%. **Membrane purification.** For the diafiltration, Amicon® Ultra-0.5 Centrifugal Filter Unit (RC, 100KDa, 3000g) were purchased from Millipore, the tools were used with mQ water twice before use. Classic dialysis against mQ water was performed with spectrapor dialysis membrane tubing (RC, 25KDa) were purchased from ThermoFisher scientific, gently washed with mQ water before use. **Complete cell culture medium** (CCM) consisted of RPMI supplemented with 10% of FBS. Au NPs were speedily added (1:10) into CMM by micropipettes and gently mixed, all the procedures were done in sterile conditions. **Physicochemical Characterization: Electron Microscopy**. The diameter of the synthesized particles was obtained from analysis of Scanning Electron Microscopy (SEM) with FEI Magellan XHR SEM, in transmission mode operated at 20 kV. Samples were prepared by drop-casting 4μL of the sample on a carbon-coated copper TEM grid and left to dry at room temperature. At least 500 particles from different regions of the grid were counted. **UV-Vis Spectroscopy**. UV-Vis spectra were acquired with a Shimadzu UV-2400 spectrophotometer. 1 mL of sample was placed in a plastic/quartz cuvette, and spectral analysis was performed in the 300−750 nm or 300-950 nm range at room temperature. Water was taken as the reference for all samples. UV-Vis absorption spectra of AuNPs is due to NPs localized surface plasmon resonance (LSPR), i.e. the collective oscillation of the metallic surface electrons, highly sensitive to the NP environment [42, 43]. The LSPR profile and maximum position strictly depend on the material, shape, and size of the NPs, as well as the refractive index (RI) of the solvent. Moreover, local RI changes, such as those induced by NP stabilizing-molecule exchange or bio-molecule interactions at the surface of the NPs produce a shift of the LSPR. Red-shifts are observed in the case of a RI increase around metal, *vice versa* a decrease produces a blue-shift. In the case of NP aggregation, considerable UV-Vis spectra changes are observed, ascribable to a near-field electromagnetic coupling. In most cases, the resonance peak of two metal NPs red-shifts and/or produces the comparison of a second peak at a higher wavelength [41]. **Size and Zeta Potential Measurements**. The hydrodynamic diameter and Z potential of the AuNPs before and after incubation in CCM were determined by Dynamic Light Scattering, and Laser Doppler Anemometry, respectively, using a Malvern Zetasizer Nano ZS instrument equipped with a light source wavelength of 532 nm and a fixed scattering angle of 173°. Diameters were reported as distribution by intensity calculated by non-negative least squares (NNLS) analysis. The software was arranged with the parameters of refractive index and adsorption coefficient of gold, and solvent viscosity of water at 25°C. **Theoretical calculation of NPs total surface area and bilayer concentration.** NPs total surface areas were calculated assuming AuNS as a perfect sphere and AuNR as a perfect cylinder, assuming as starting radius and height the values measured by STEM and the concentration of Au used to perform the synthesis. The theoretical CTAB concentration that formed

the bilayer on the AuNPs was calculated dividing the total surface areas of NPs for the surfactant headgroup area (0.64nm^2) [72] multiplied for two. In the case of AuNS was also calculated taking into consideration that the radius where it is positioned the second layer is increased by the first one, considering an increment of the diameters of 1.5+1.5nm (length of CTAB) [25]. **Analysis of CTAB in aqueous solutions by the Ion-Pair method.** Quantification of CTAB was performed by adapting the protocol developed by C. Adura et al. [73]. Briefly, 5 mL of $CHCl_3$ was added to a 15 ml lab glass. The colloidal solution of nanoparticles was centrifuged until all the nanoparticles were precipitated in the form of pellets. 1 ml of the supernatant was added of 1 ml of 500 µM bromophenol blue sodium salt (BPB) water solution. The sample was stirred vigorously (1000 r.p.m) for 45 minutes, maintaining the glass vial completely seals in order to maintain the volume constant. The aqueous phase must has an excess of BPB. If the aqueous phase becomes transparent during the procedure, the analysis is invalid because CTAB concentration is out of range. The samples were leaved without stirring for 5 minutes to separate the organic phase. The organic phase was extract using glass pipettes and read in the spectrophotometer between 500-700nm. The CTAB concentration was calculated in µM using the obtained absorbance at 606nm and the equation of the previous prepared calibration curve. Has to be take into account that the final result is diluted 1:5.

Supporting Information Description

LSPR, Z potential and stability changes observed in the AuNPs purification by dialysis; Over time Water/Octanol partition of AuNS at the different washing steps; ligand exchange of AuNS@PVP with CTAB.

Author information

Corresponding Author
*E-mail: victor.puntes@icn2.cat

Acknowledgements

We acknowledge financial support from the Pandora European Training Network (GA-671881) funded in the framework of H2020Marie Skłodowska-Curie ITN programme; the doctorate in

Chemistry and Materials Science at the Autonomous University of Barcelona (UAB). N.G.B. acknowledges financial support by MINECO through the Ramon y Cajal program (RYC-2012-10991).

References

1. Sperling, R.A., et al., *Biological applications of gold nanoparticles.* Chemical Society Reviews, 2008. **37**(9): p. 1896-1908.
2. Ghosh, P., et al., *Gold nanoparticles in delivery applications.* Advanced drug delivery reviews, 2008. **60**(11): p. 1307-1315.
3. Hvolbæk, B., et al., *Catalytic activity of Au nanoparticles.* Nano Today, 2007. **2**(4): p. 14-18.
4. Chen, Y., Y. Xianyu, and X. Jiang, *Surface modification of gold nanoparticles with small molecules for biochemical analysis.* Accounts of chemical research, 2017. **50**(2): p. 310-319.
5. Clavero, C., *Plasmon-induced hot-electron generation at nanoparticle/metal-oxide interfaces for photovoltaic and photocatalytic devices.* Nature Photonics, 2014. **8**(2): p. 95.
6. Bastús, N.G., et al., *The reactivity of colloidal inorganic nanoparticles*, in *The Delivery of Nanoparticles*. 2012, InTech.
7. Dreaden, E.C., et al., *The golden age: gold nanoparticles for biomedicine.* Chemical Society Reviews, 2012. **41**(7): p. 2740-2779.
8. Takahashi, H., et al., *Modification of gold nanorods using phosphatidylcholine to reduce cytotoxicity.* Langmuir, 2006. **22**(1): p. 2-5.
9. Jana, N.R., L. Gearheart, and C.J. Murphy, *Seeding growth for size control of 5− 40 nm diameter gold nanoparticles.* Langmuir, 2001. **17**(22): p. 6782-6786.
10. Murphy, C.J., et al., *Anisotropic metal nanoparticles: synthesis, assembly, and optical applications*. 2005, ACS Publications.
11. Millstone, J.E., G.S. Métraux, and C.A. Mirkin, *Controlling the edge length of gold nanoprisms via a seed-mediated approach.* Advanced Functional Materials, 2006. **16**(9): p. 1209-1214.
12. Trigari, S., et al., *Synthesis and modelling of gold nanostars with tunable morphology and extinction spectrum.* Journal of Materials Chemistry, 2011. **21**(18): p. 6531-6540.
13. Lohse, S.E., et al., *Nanomaterial probes in the environment: gold nanoparticle soil retention and environmental stability as a function of surface chemistry.* ACS Sustainable Chemistry & Engineering, 2017. **5**(12): p. 11451-11458.
14. Lee, J., et al., *In vitro toxicity testing of nanoparticles in 3D cell culture.* Small, 2009. **5**(10): p. 1213-1221.
15. Bhamidipati, M. and L. Fabris, *Multiparametric assessment of gold nanoparticle cytotoxicity in cancerous and healthy cells: the role of size, shape, and surface chemistry.* Bioconjugate chemistry, 2017. **28**(2): p. 449-460.
16. Connor, E.E., et al., *Gold nanoparticles are taken up by human cells but do not cause acute cytotoxicity.* Small, 2005. **1**(3): p. 325-327.
17. Alkilany, A.M., et al., *Cellular uptake and cytotoxicity of gold nanorods: molecular origin of cytotoxicity and surface effects.* small, 2009. **5**(6): p. 701-708.
18. Cheng, W., S. Dong, and E. Wang, *Synthesis and self-assembly of cetyltrimethylammonium bromide-capped gold nanoparticles.* Langmuir, 2003. **19**(22): p. 9434-9439.
19. Coppola, L., et al., *Structural changes in CTAB/H2O mixtures using a rheological approach.* Physical Chemistry Chemical Physics, 2004. **6**(9): p. 2364-2372.

20. Kuperkar, K., et al., *Formation and growth of micelles in dilute aqueous CTAB solutions in the presence of NaNO3 and NaClO3.* Journal of Surfactants and Detergents, 2010. **13**(3): p. 293-303.
21. del Mar Graciani, M., et al., *Water− N, N-dimethylformamide alkyltrimethylammonium bromide micellar solutions: thermodynamic, structural, and kinetic studies.* Langmuir, 2005. **21**(8): p. 3303-3310.
22. Shikata, T., H. Hirata, and T. Kotaka, *Micelle formation of detergent molecules in aqueous media: viscoelastic properties of aqueous cetyltrimethylammonium bromide solutions.* Langmuir, 1987. **3**(6): p. 1081-1086.
23. Danov, K.D., P.A. Kralchevsky, and K.P. Ananthapadmanabhan, *Micelle–monomer equilibria in solutions of ionic surfactants and in ionic–nonionic mixtures: A generalized phase separation model.* Advances in colloid and interface science, 2014. **206**: p. 17-45.
24. Nikoobakht, B. and M.A. El-Sayed, *Evidence for bilayer assembly of cationic surfactants on the surface of gold nanorods.* Langmuir, 2001. **17**(20): p. 6368-6374.
25. Gómez-Graña, S., et al., *Surfactant (bi) layers on gold nanorods.* Langmuir, 2011. **28**(2): p. 1453-1459.
26. Burrows, N.D., et al., *Surface chemistry of gold nanorods.* Langmuir, 2016. **32**(39): p. 9905-9921.
27. Lee, S., et al., *Structural transition in the surfactant layer that surrounds gold nanorods as observed by analytical surface-enhanced Raman spectroscopy.* Langmuir, 2011. **27**(24): p. 14748-14756.
28. Ito, E., et al., *Potential use of cetrimonium bromide as an apoptosis-promoting anti-cancer agent for head and neck cancer.* Molecular pharmacology, 2009.
29. Indrasekara, A.S.D., R.C. Wadams, and L. Fabris, *Ligand exchange on gold nanorods: going back to the future.* Particle & Particle Systems Characterization, 2014. **31**(8): p. 819-838.
30. Wang, S., et al., *Challenge in understanding size and shape dependent toxicity of gold nanomaterials in human skin keratinocytes.* Chemical physics letters, 2008. **463**(1-3): p. 145-149.
31. Sethi, M., G. Joung, and M.R. Knecht, *Stability and electrostatic assembly of Au nanorods for use in biological assays.* Langmuir, 2008. **25**(1): p. 317-325.
32. Goris, B., et al., *Atomic-scale determination of surface facets in gold nanorods.* Nature materials, 2012. **11**(11): p. 930.
33. Grzelczak, M., et al., *Shape control in gold nanoparticle synthesis.* Chemical Society Reviews, 2008. **37**(9): p. 1783-1791.
34. Piella, J., et al., *Probing the surface reactivity of nanocrystals by the catalytic degradation of organic dyes: the effect of size, surface chemistry and composition.* Journal of Materials Chemistry A, 2017. **5**(23): p. 11917-11929.
35. Carbó-Argibay, E., et al., *The Crystalline Structure of Gold Nanorods Revisited: Evidence for Higher-Index Lateral Facets.* Angewandte Chemie International Edition, 2010. **49**(49): p. 9397-9400.
36. Chen, H., et al., *Gold nanorods and their plasmonic properties.* Chemical Society Reviews, 2013. **42**(7): p. 2679-2724.
37. Cosgrove, T., *Colloid science: principles, methods and applications*. 2010: John Wiley & Sons.
38. Abbott, S. and N. Holmes, *Nanocoatings: Principles and Practice: From Research to Production*. 2013: DEStech Publications, Inc.
39. Bastus, N.G., J. Piella, and V. Puntes, *Quantifying the Sensitivity of Multipolar (Dipolar, Quadrupolar, and Octapolar) Surface Plasmon Resonances in Silver Nanoparticles: The Effect of Size, Composition, and Surface Coating.* Langmuir, 2016. **32**(1): p. 290-300.

40. Pastoriza-Santos, I., et al., *Optical properties of metal nanoparticle coated silica spheres: a simple effective medium approach.* Physical Chemistry Chemical Physics, 2004. **6**(21): p. 5056-5060.
41. Sepúlveda, B., et al., *LSPR-based nanobiosensors.* nano today, 2009. **4**(3): p. 244-251.
42. Willets, K.A. and R.P. Van Duyne, *Localized surface plasmon resonance spectroscopy and sensing.* Annu. Rev. Phys. Chem., 2007. **58**: p. 267-297.
43. Liz-Marzán, L.M., *Tailoring surface plasmons through the morphology and assembly of metal nanoparticles.* Langmuir, 2006. **22**(1): p. 32-41.
44. Makino, K. and H. Ohshima, *Electrophoretic mobility of a colloidal particle with constant surface charge density.* Langmuir, 2010. **26**(23): p. 18016-18019.
45. Bastús, N.G., J. Piella, and V. Puntes, *Quantifying the sensitivity of multipolar (dipolar, quadrupolar, and octapolar) surface plasmon resonances in silver nanoparticles: The effect of size, composition, and surface coating.* Langmuir, 2015. **32**(1): p. 290-300.
46. Murphy, C.J., et al., *Gold nanorod crystal growth: from seed-mediated synthesis to nanoscale sculpting.* Current Opinion in Colloid & Interface Science, 2011. **16**(2): p. 128-134.
47. Sangster, J., *Octanol-water partition coefficients: fundamentals and physical chemistry*. 1997: John Wiley & Sons.
48. Klíčová, L.u., et al., *CTAB/water/chloroform reverse micelles: a closed or open association model?* Langmuir, 2012. **28**(43): p. 15185-15192.
49. Miller, S., D. Dykes, and H. Polesky, *A simple salting out procedure for extracting DNA from human nucleated cells.* Nucleic acids research, 1988. **16**(3): p. 1215.
50. Ojea-Jiménez, I., et al., *Facile preparation of cationic gold nanoparticle-bioconjugates for cell penetration and nuclear targeting.* ACS nano, 2012. **6**(9): p. 7692-7702.
51. Yang, J., et al., *Organic solvent dependence of plasma resonance of gold nanorods: A simple relationship.* Chemical physics letters, 2005. **416**(4-6): p. 215-219.
52. BaniáYaseen, A., *Facile phase transfer of gold nanoparticles from aqueous solution to organic solvents with thiolated poly (ethylene glycol).* RSC Advances, 2014. **4**(95): p. 52676-52679.
53. López-Millán, A., et al., *Aqueous-Organic Phase Transfer of Gold and Silver Nanoparticles Using Thiol-Modified Oleic Acid.* Applied Sciences, 2017. **7**(3): p. 273.
54. Imura, Y., et al., *Water and Organic Solvent Dispersible Gold Nanorods that are pH Responsive.* ChemistrySelect, 2016. **1**(17): p. 5404-5408.
55. Krpetić, Z.e., et al., *Negotiation of intracellular membrane barriers by TAT-modified gold nanoparticles.* ACS nano, 2011. **5**(6): p. 5195-5201.
56. Nel, A., et al., *Toxic potential of materials at the nanolevel.* science, 2006. **311**(5761): p. 622-627.
57. Dobrovolskaia, M.A. and S.E. McNeil, *Immunological properties of engineered nanomaterials.* Nature nanotechnology, 2007. **2**(8): p. 469.
58. Tenzer, S., et al., *Rapid formation of plasma protein corona critically affects nanoparticle pathophysiology.* Nature nanotechnology, 2013. **8**(10): p. 772.
59. Saha, K., et al., *Regulation of macrophage recognition through the interplay of nanoparticle surface functionality and protein corona.* ACS nano, 2016. **10**(4): p. 4421-4430.
60. Di Silvio, D., et al., *Effect of protein corona magnetite nanoparticles derived from bread in vitro digestion on Caco-2 cells morphology and uptake.* The international journal of biochemistry & cell biology, 2016. **75**: p. 212-222.
61. Monopoli, M.P., et al., *Physical− chemical aspects of protein corona: relevance to in vitro and in vivo biological impacts of nanoparticles.* Journal of the American Chemical Society, 2011. **133**(8): p. 2525-2534.
62. Lundqvist, M., et al., *Nanoparticle size and surface properties determine the protein corona with possible implications for biological impacts.* Proceedings of the National Academy of Sciences, 2008.

63. Wang, L., et al., *Revealing the binding structure of the protein corona on gold nanorods using synchrotron radiation-based techniques: understanding the reduced damage in cell membranes.* Journal of the American Chemical Society, 2013. **135**(46): p. 17359-17368.
64. Alkilany, A.M. and C.J. Murphy, *Toxicity and cellular uptake of gold nanoparticles: what we have learned so far?* Journal of nanoparticle research, 2010. **12**(7): p. 2313-2333.
65. Dominguez-Medina, S., et al., *Adsorption and unfolding of a single protein triggers nanoparticle aggregation.* ACS nano, 2016. **10**(2): p. 2103-2112.
66. Dennison, J.M., et al., *Protein Adsorption to Charged Gold Nanospheres as a Function of Protein Deformability.* Langmuir, 2017. **33**(31): p. 7751-7761.
67. Drescher, D., et al., *SERS reveals the specific interaction of silver and gold nanoparticles with hemoglobin and red blood cell components.* Physical Chemistry Chemical Physics, 2013. **15**(15): p. 5364-5373.
68. Vlasova, I., V. Zhuravleva, and A. Saletskii, *Denaturation of bovine serum albumin under the action of cetyltrimethylammonium bromide, according to data from fluorescence analysis.* Russian Journal of Physical Chemistry A, 2013. **87**(6): p. 1027-1034.
69. Jahn, T.R. and S.E. Radford, *Folding versus aggregation: polypeptide conformations on competing pathways.* Archives of biochemistry and biophysics, 2008. **469**(1): p. 100-117.
70. Casals, E., et al., *Time evolution of the nanoparticle protein corona.* ACS nano, 2010. **4**(7): p. 3623-3632.
71. Barbero, F., et al. *Formation of the Protein Corona: The Interface between Nanoparticles and the Immune System*. in *Seminars in immunology*. 2017. Elsevier.
72. Zhao, F., et al., *Determination of surfactant molecular volume by atomic force microscopy.* Colloid Journal, 2006. **68**(6): p. 784-787.
73. Adura, C., et al., *ION PAIR METHOD TO DETERMINE THE CTAB CONTENT IN GOLD NANORODS SAMPLES.* Journal of the Chilean Chemical Society, 2014. **59**(4): p. 2701-2704.

Table of Contents

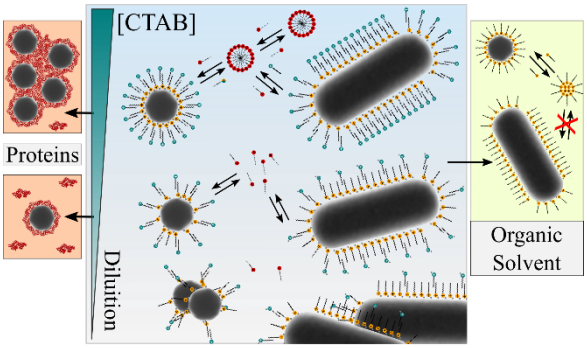

For Table of Contents Only